ISPRS Open Journal of Photogrammetry and Remote Sensing 8 (2023) 100034

Contents lists available at ScienceDirect

ISPRS Open Journal of Photogrammetry and Remote Sensing

journal homepage: www.journals.elsevier.com/isprs-open-journal-of-photogrammetry-and-remote-sensing

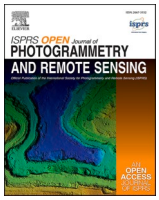

UAV-based reference data for the prediction of fractional cover of standing deadwood from Sentinel time series

Felix Schiefer [a,*], Sebastian Schmidtlein [a], Annett Frick [b], Julian Frey [c], Randolf Klinke [b], Katarzyna Zielewska-Büttner [d], Samuli Junttila [e], Andreas Uhl [f], Teja Kattenborn [g,h]

[a] Karlsruhe Institute of Technology (KIT), Institute of Geography and Geoecology, Kaiserstraße 12, 76131, Karlsruhe, Germany
[b] Luftbild Umwelt Planung GmbH (LUP), 14469, Potsdam, Germany
[c] University of Freiburg, Forest Growth and Dendroecology, 79106, Freiburg, Germany
[d] Forest Research Institute (FVA) Baden-Württemberg, Department of Forest Nature Conservation, 79100, Freiburg, Germany
[e] University of Eastern Finland, School of Forest Sciences, 80101, Joensuu, Finland
[f] Forest Research Institute (FVA) Baden-Württemberg, Department of Biometry and Informatics, 79100, Freiburg, Germany
[g] Remote Sensing Centre for Earth System Research (RSC4Earth), Leipzig University, Germany
[h] German Centre for Integrative Biodiversity Research (iDiv), Halle-Jena-Leipzig, Germany

ARTICLE INFO

Keywords:
Reference data
Standing deadwood
Deep learning
Tree mortality
Upscaling

ABSTRACT

Increasing tree mortality due to climate change has been observed globally. Remote sensing is a suitable means for detecting tree mortality and has been proven effective for the assessment of abrupt and large-scale stand-replacing disturbances, such as those caused by windthrow, clear-cut harvesting, or wildfire. Non-stand replacing tree mortality events (e.g., due to drought) are more difficult to detect with satellite data – especially across regions and forest types. A common limitation for this is the availability of spatially explicit reference data. To address this issue, we propose an automated generation of reference data using uncrewed aerial vehicles (UAV) and deep learning-based pattern recognition. In this study, we used convolutional neural networks (CNN) to semantically segment crowns of standing dead trees from 176 UAV-based very high-resolution (<4 cm) RGB-orthomosaics that we acquired over six regions in Germany and Finland between 2017 and 2021. The local-level CNN-predictions were then extrapolated to landscape-level using Sentinel-1 (i.e., backscatter and interferometric coherence), Sentinel-2 time series, and long short term memory networks (LSTM) to predict the cover fraction of standing deadwood per Sentinel-pixel. The CNN-based segmentation of standing deadwood from UAV imagery was accurate (F1-score = 0.85) and consistent across the different study sites and years. Best results for the LSTM-based extrapolation of fractional cover of standing deadwood using Sentinel-1 and -2 time series were achieved using all available Sentinel-1 and –2 bands, kernel normalized difference vegetation index (kNDVI), and normalized difference water index (NDWI) (Pearson's r = 0.66, total least squares regression slope = 1.58). The landscape-level predictions showed high spatial detail and were transferable across regions and years. Our results highlight the effectiveness of deep learning-based algorithms for an automated and rapid generation of reference data for large areas using UAV imagery. Potential for improving the presented upscaling approach was found particularly in ensuring the spatial and temporal consistency of the two data sources (e.g., co-registration of very high-resolution UAV data and medium resolution satellite data). The increasing availability of publicly available UAV imagery on sharing platforms combined with automated and transferable deep learning-based mapping algorithms will further increase the potential of such multi-scale approaches.

1. Introduction

Tree mortality has immense consequences for forestry, environmental protection, and ecosystem services and it is increasing globally due to changes in climate and related extreme events (Allen et al., 2010; Hartmann et al., 2022). For instance, in Europe recent excess rates of tree mortality could be related to intense drought events in the years 2018 and 2019 (Bastos et al., 2021; Senf et al., 2020, 2021). Still, the

* Corresponding author.
E-mail address: felix.schiefer@kit.edu (F. Schiefer).

https://doi.org/10.1016/j.ophoto.2023.100034
Received 11 October 2022; Received in revised form 27 February 2023; Accepted 6 March 2023
Available online 8 March 2023

mechanisms and factors explaining excess rates of tree mortality are not fully understood (Hartmann et al., 2018). For instance, tree mortality varies widely depending on tree species composition, forest management, and site conditions. Furthermore, drivers of tree mortality, such as climate extremes, have complex spatial and temporal patterns. They may even act in compound events, such as consecutive drought years, late spring frosts, and subsequent insect and pathogen outbreaks (Hartmann et al., 2018; Huang et al., 2020; Zscheischler et al., 2020). To understand recent excess rates of tree mortality or to develop methods to forecast such events in the future, we need spatially and temporally continuous information on tree mortality (Hartmann et al., 2022). However, detecting and quantifying tree mortality over large spatial and temporal scales remains challenging.

Remote sensing is being successfully applied for the detection of abrupt and large-scale stand replacing disturbances, such as those caused by windthrow, wildfire, or clear-cut harvesting, to be feasible at regional and global scales at a 30 m spatial resolution (Hansen et al., 2013; Senf and Seidl, 2021; White et al., 2017). Less focus has been given to non-stand replacing disturbances, where tree mortality occurs more subtle and scattered across landscapes, affecting only individual trees or smaller groups. For example, this type of disturbance dynamics can be triggered by drought or insects (Coops et al., 2020), particularly in the initial phase of disturbance. Such patterns are critical to our understanding of tree mortality dynamics, but cannot be accurately detected at 30 m spatial resolution (Frolking et al., 2009; Senf et al., 2021; Trumbore et al., 2015).

Various studies have demonstrated the potential of higher spatial resolution satellite data (Liu et al., 2021) or aerial (ortho-)images (Chiang et al., 2020; Fricker et al., 2019; Jiang et al., 2019; Meddens et al., 2011; Monahan et al., 2022; Sylvain et al., 2019; Zielewska--Büttner et al., 2020) to explicitly detect tree mortality. However, such datasets are usually limited to small extents, are expensive to acquire, and are often only acquired sporadically, which limits the spatially and temporally systematic detection of deadwood. Other studies have attempted to compensate for the coarse resolution of Earth observation satellites by using spectral information to indirectly track tree mortality. For example, tree mortality was approximated from relative changes of spectral indices (Bárta et al., 2021; Thonfeld et al., 2022) or biochemical and biophysical traits obtained from radiative transfer models (Ali et al., 2021). However, such spectral indices or traits also vary depending on a number of factors unrelated to tree mortality (e.g. species composition, forest structure), but in a confounding way (Frolking et al., 2009; Glenn et al., 2008; Xue and Su, 2017). Such approaches can only provide indirect information on tree mortality and therefore do not explicitly indicate whether tree crowns are dead or not.

Explicit detection and quantification of tree mortality, for instance in terms of cover of dead tree crowns per area, requires spatially explicit reference data for model calibration and validation. However, such reference datasets are scarce and costly to obtain, and are therefore one of the most limiting factors for conducting large-scale remote sensing analyses for deadwood detection (Frolking et al., 2009; McDowell et al., 2015; Schuldt et al., 2020; Trumbore et al., 2015). Moreover, existing *in situ* reference datasets, such as those from national forest inventories, are not explicitly designed to study or quantify tree mortality, and often do not provide an estimate of canopy cover, which limits their usability for remote sensing approaches.

Several authors have highlighted this lack of ground reference data and emphasized the need for global reference databases on tree mortality following standardized protocols (Allen et al., 2010; Buras et al., 2020; McDowell et al., 2015; Schuldt et al., 2020). Initiatives such as the International Tree Mortality Network are compiling harmonized global datasets on field-based research plots to study tree mortality (Hammond et al., 2022). But even with a well curated dataset of global coverage, the integration of ground-based reference data with Earth observation satellite data is challenging: Pixel sizes of suitable Earth observation satellite missions, such as Landsat or Sentinel, do not enable to resolve individual trees and, hence, hamper the link with ground reference observations. In addition, properties typically measured on the ground (e.g., tree stem coordinates) do not necessarily allow for a spatially explicit link to what satellites 'see' from a bird's eye perspective (e.g., tree canopy reflectance) (Pause et al., 2016; Schiefer et al., 2020). Moreover, dense canopy cover or complex topography can considerably limit GNSS accuracies of ground measurements, making reliable geopositioning in the field even more difficult (Kaartinen et al., 2015; Valbuena et al., 2010). Overall, both the quality and quantity of common reference data do not facilitate the mapping of tree mortality at large spatial scales with Earth observation data.

These practical limitations and the general scarcity of ground reference data on tree mortality may be compensated by uncrewed aerial vehicles (UAV) (Alvarez-Vanhard et al., 2021; Kattenborn et al., 2019; Liu et al., 2021; Schiefer et al., 2020). The very-high spatial resolution of UAV RGB imagery enables precise segmentation of dead tree crowns, and the flexible deployment of UAVs further enables efficient detection of tree mortality events over large and even inaccessible areas. Especially in combination with recent advances in pattern recognition and deep learning, such as Convolutional Neural Networks (CNN), very accurate results for crown segmentation of standing dead trees have been demonstrated (Chiang et al., 2020; Sani-Mohammed et al., 2022; Schiefer et al., 2020). Because such predictions also emerge from the bird's eye perspective, they may be readily used for subsequent satellite-based and thus large-scale analyses (Kattenborn et al., 2019). The concerted use of UAVs and CNNs and their efficiency enable the generation of ample amounts of reference data over large areas and multiple years. This may greatly facilitate the training of robust satellite-based models that are transferable across temporal, spatial, or environmental conditions.

Hence, to compensate for the lack of ground reference data on tree mortality, we propose an upscaling approach in which fine-scaled patterns in UAV imagery are harnessed to create ample reference data at local scales for training models that predict standing deadwood at the landscape-scale using multitemporal and multispectral information of satellite data. In doing so, we seek to answer the following research questions: *(1)* Are CNN-based predictions of standing deadwood from UAV imagery robust across a wide range of forest stand characteristics and over multiple years? *(2)* Can these CNN-based predictions from UAV imagery serve as reference data to accurately predict fractional cover of standing deadwood with Sentinel imagery at 10 m spatial resolution? *(3)* Is this upscaling approach transferable across regions and different years?

2. Material and methods

The workflow of this study consisted of a local-level and a landscape-level part (Fig. 1). In the local-level part we tested the combination of UAV RGB imagery and CNN-based pattern recognition for an automated extraction of standing dead tree crowns. We then upscaled these UAV-based segmentations of standing dead trees to fractional cover at the landscape-level using satellite-based time series analysis. For this upscaling, we used Sentinel-1 and Sentinel-2 time series together with a long short-term memory network (LSTM).

2.1. Study area and UAV data acquisition

This study comprised a set of UAV data acquisitions from the six study regions Southern Black Forest, Northern Black Forest, Dresden Heath, Karlsruhe-Bretten, and Hainich National Park in Germany, as well as Helsinki, Finland (Fig. 2). The sites comprise a large heterogeneity in terms of species composition and forest structure, which results from different environments and forest management (see site information in Table 1).

In total, we acquired orthoimages over 176 sites across the six regions. For each site, we acquired UAV-based RGB photographs and

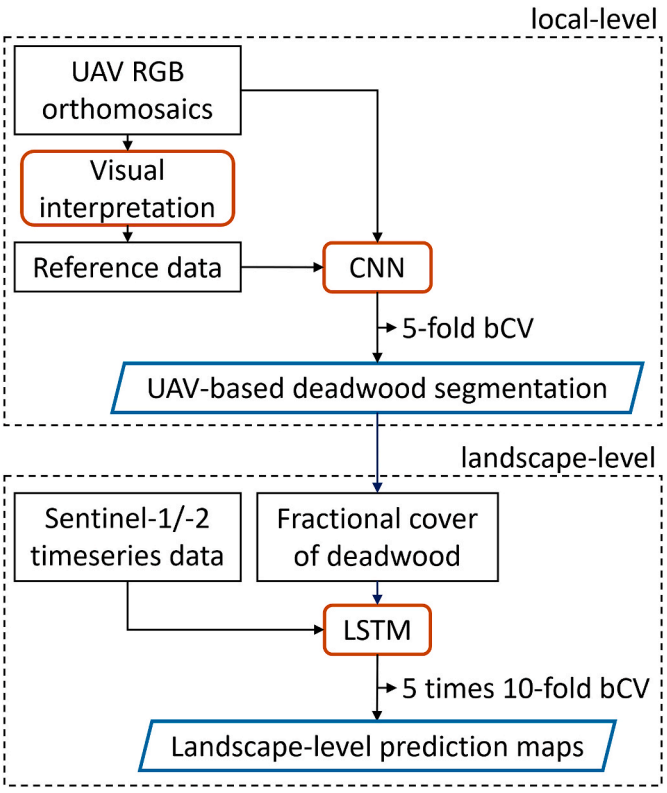

Fig. 1. Schematic workflow of the upscaling approach. CNN-based deadwood segmentation from UAV RGB orthomosaics (local-level) are upscaled to fractional cover of standing deadwood using Sentinel-1/-2 timeseries date and an LSTM model (landscape-level). bCV: block cross-validation.

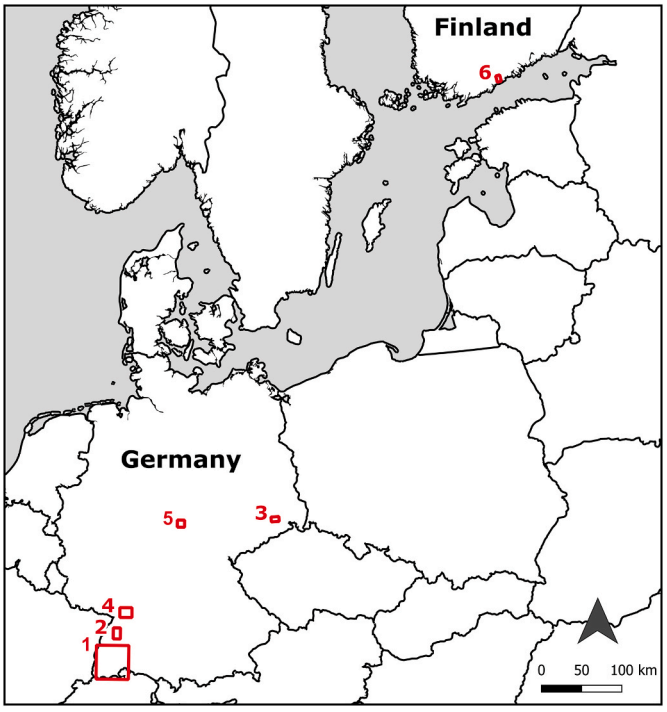

Fig. 2. The six study regions: (1) Southern Black Forest, (2) Black Forest, (3) Dresden Heath, (4) Karlsruhe-Bretten, (5) Hainich National Park, and (6) Helsinki.

derived orthomosaics using Structure-from-Motion photogrammetric processing chains (details see e.g., Schiefer et al. (2020)). The UAV orthoimagery was acquired with different UAV platforms, camera systems, flight planning software, acquisition settings, and photogrammetric workflows for orthoimage generation (an overview of the different settings for each dataset is given in Table 1). The orthoimagery covered a total area of 727.33 ha and the spatial extent of the individual orthomosaics ranged from 1.29 to 32.72 ha. The ground sampling distance (GSD) ranged from 0.60 to 3.39 cm and was resampled to a common pixel size of 4 cm.

2.2. CNN-based segmentation of standing deadwood at local level

For mapping dead trees at the local level, we choose a semantic segmentation approach that allows to predict dead tree crowns at the original pixel-size of the UAV imagery. The training of common CNN segmentation models requires image data that is fully labeled in form of masks. We prepared binary masks (absence/presence of dead tree crowns) by delineating standing dead trees from all the available orthomosaics using visual interpretation in ArcGIS v.10.6.1 (ESRI, Redlands, USA). Labeling all sites is not a requirement of the CNN approach but is necessary to obtain a comprehensive picture of the model performance across sites and years. We delineated trees and branches that were clearly identifiable as dead, as indicated by degraded, discolored, or entirely absent foliage. Trees that were damaged but still had green foliage (e.g., green attack after bark beetle infestation) were not included, which facilitates visual interpretation and ensures its robustness.

For the CNN model training, we cropped the orthomosaics and the corresponding masks into 40451 non-overlapping tiles of 256 × 256 pixels (edge length of 10.24 m). We used the U-net CNN architecture (Ronneberger et al., 2015) to automatically segment standing dead trees in the orthomosaics. The U-net features an encoding path to capture spatial features and their context and a decoding path to map the resembled information to the original image dimensions. Here, we used five blocks in the encoding path, each consisting of two 3 × 3 convolutions, followed by batch normalization, a linear rectifier unit activation, and 2 × 2 max-pooling operation with a striding of two. In these blocks, the convolutional layers had a depth of 1024, 512, 256, 128, and 64 layers for the encoder path and the same but in reverse order for the decoder path. A detailed description of the utilized U-net architecture can be found in Schiefer et al. (2020). Here, we used a sigmoid activation in the final layer. The CNN was trained with a batch size of 32 tiles over 60 epochs using binary cross entropy loss and RMSprop optimizer with a learning rate of 10^{-4}. For model regularization, we augmented the training tiles using random horizontal and vertical flips and random changes in image brightness (90–110%), contrast (80–120%), and saturation (80–120%), thereby increasing the size of the training dataset to twice its size.

To avoid biased model performance estimates due to spatial dependence between training and test data, we assessed the CNN model performance using five-fold spatial block cross-validation (Kattenborn et al., 2022). We randomly split the image tiles from the study sites (n = 176) into five folds, thereby ensuring, that from each of the six study regions at least one site was included. In each step, the sites from one fold served as an independent test set, and the sites from the remaining four folds were split into 80% training and 20% validation set. Using the independent test set, the final model performance was assessed on a per-pixel level based on precision, recall, and F1-score (the harmonic mean of the first two).

2.3. Mapping deadwood cover fractions at landscape level using satellite time series

2.3.1. Satellite time series

For the extrapolation to landscape-level using satellite data and

Table 1
Summary of the regions, sites, and the corresponding UAV acquisitions.

Study region	Site information			UAV data			
	Number of sites n = 176	Forest type (management)	Dominant tree species	UAV system (camera)	GSD [cm]	covered area [ha]	year(s) of acquisition
Southern Black Forest	141	mixed and coniferous (managed for timber production)	*Picea abies* L., *Fagus sylvatica* L., *Abies alba* Mill.	HiSystems MK Okto-XL (Sony Alpha 7R)	0.65–3.12	375.13	2017–2021
Northern Black Forest	14	mixed and coniferous (managed for timber production; unmanaged)	*Picea abies, Abies alba, Fagus sylvatica*	DJI Phantom 4 Pro (FC6310S)	1.08–2.68	169.00	2019, 2021
Dresden Heath	8	mixed and coniferous (managed for timber production)	*Picea abies, Fagus sylvatica, Quercus spec., Betula pendula* (Roth)	DJI Phantom 4 Pro (FC6310S)	1.92–2.60	46.41	2021
Karlsruhe-Bretten	6	mixed (managed for timber production)	*Pinus sylvestris* L., *Quercus rubra* L., *Carpinus betulus* L., *Fagus sylvatica*	HiSystems MK Okto-XL (Canon 100D)	1.62–2.76	37.57	2019
Hainich National Park	4	mixed deciduous (unmanaged)	*Fagus sylvatica*	DJI Phantom 4 Pro (FC6310S)	0.80–1.35	8.58	2019
Helsinki	3	mixed and coniferous (managed for path safety)	*Picea abies, Pinus sylvestris, Betula pendula, Populus tremula* L.	DJI Phantom 4 Pro (FC6310S)	2.97–3.39	90.63	2020

LSTM, we used the CNN-based segmentations (not the manually created masks) from high resolution UAV imagery and calculated the fractional cover (%) of standing deadwood per Sentinel grid cell using a superimposed Sentinel-2 pixel grid (10 m resolution). Summary statistics for all sites are given in the Appendix. To map the fractional cover of standing dead trees at the landscape level, we extracted time series from Sentinel-1 and Sentinel-2 images acquired between October 1, 2015 and September 30, 2021. For Sentinel-2, we used the Level-2A product that provides atmospheric- and terrain-corrected Bottom Of Atmosphere (BOA) reflectance images (Main-Knorn et al., 2017). We selected bands with 10 m GSD (i.e., B2 blue, B3 green, B4 red, and B8 near infrared), 20 m GSD (i.e., B5–B7 red edge, and B11–B12 short-wavelength infrared), and two with 60 m GSD (i.e., B1 aerosols and B9 water vapor). In addition to the spectral bands, we calculated the kernel normalized difference vegetation index (kNDVI, Camps-Valls et al., 2021) using the red (B4) and near infrared (B8) bands, and normalized difference water index (NDWI, Gao, 1996) using the narrow near infrared (B8A) and short wave infrared (B11) bands. Pixel values with kNDVI <0.1 were masked out from the Sentinel-2 bands, as they primarily represent atmospheric water and clouds.

For Sentinel-1, we selected Level-1 Ground Range Detected (GRD) and Single Look Complex (SLC) data from Interferometric Wide Swath Mode (IW) in dual polarization of type VV + VH. We used the Copernicus Analysis Ready Data (CARD) processors that provide terrain-corrected backscatter (CARD-BS) and interferometric coherence (CARD-COH6) data. The CARD-BS processor consists of application of orbit file, removal of border and thermal noise, radiometric calibration, and terrain correction. The CARD-COH6 processor consists of application of orbit file, TOPSAR split, back-geocoding, coherence, TOPSAR deburst, TOPSAR merge, multilooking, and terrain correction. For terrain correction the Copernicus DEM 30m elevation data were used. For both Sentinel-1 and -2, all spectral bands were resampled to 10 m spatial resolution using nearest-neighbor interpolation. We linearly interpolated missing values and converted the time series to 7-day intervals using arithmetic mean. Non-forested areas according to the Sentinel-2 Global Land Cover (S2GLC) map (Malinowski et al., 2020) were excluded from further analysis. All satellite images were accessed and preprocessed using Copernicus Data and Information Access Service (DIAS) via the CREODIAS platform (CloudFerro, Warsaw, Poland).

2.3.2. LSTM modelling

We used a long short-term memory network (LSTM) to predict fractional cover of standing deadwood based on the Sentinel-1 and Sentinel-2 time series. As a baseline to the deep learning method, we trained random forest models (Breiman, 2001), but these models performed worse (see Appendix).

LSTM is a special kind of recurrent neural network (RNN) capable of learning long-term dependencies from sequences of data without suffering from the vanishing or exploding gradient problem that can occur when training RNN (Hochreiter and Schmidhuber, 1997). LSTM units take temporal dependencies into account by controlling the network memory (or memory cell) using three sigmoid gate units (σ): a forget gate, an input gate, and an output gate (Fig. 3). Depending on the output of the previous cell (h_{t-1}) and the current input (x_t) the forget gate controls whether the previous memory cell state (C_{t-1}) will be kept by means of a sigmoid function. The input gate, similarly, controls which part of the memory cell will be updated using a sigmoid function, combined with a tanh function that creates weights that are then used to update the new cell state (C_t). Finally, the output (h_t) is determined by the output gate that decides which information of the cell state will be forwarded by means of a sigmoid function and a tanh function that scales the output between −1 and 1.

Using a bidirectional implementation of LSTM, the network trains in both time directions, thereby learning temporal dependencies from past and future time steps (Schuster and Paliwal, 1997). We used two bidirectional LSTM layers of 100 LSTM units each, followed by a fully connected layer and a sigmoid activation that predicts the final class probabilities.

We tested four different input band sets to the LSTM, namely only Sentinel-2 (S2), Sentinel-1 and Sentinel-2 (S1+S2), Sentinel-2 and

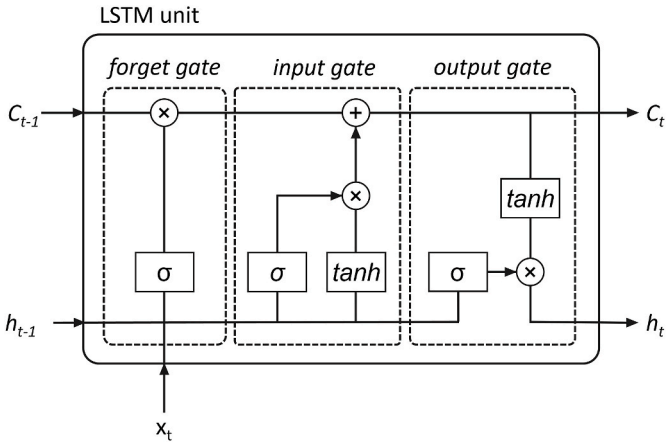

Fig. 3. Structure of an LSTM unit.

vegetation indices (S2+VI) and the combination of all available data (S1+S2+VI). We assessed the predictive performance of the LSTM models using a five times repeated ten-fold spatial block cross-validation. Here, the blocks were corresponding to the individual sites (an area covered by an individual orthomosaic). In each repetition, we randomly split the data on a site-basis (n = 176) into ten folds. In each cross-validation step, data from one fold served as independent test data and data from the remaining nine folds were split into 80% training and 20% validation data. Every LSTM model was trained for 150 epochs with a batch size of 64 using Adam optimizer. A subset (n = 6300) was sampled from the entire dataset to ensure a balanced distribution of fractional coverage values (0–100%). Because the spectral signal of bare ground can be similar to that of dead tree canopies, we added such observations (i.e., open forest floor and sparsely vegetated areas) delineated from national aerial surveys to avoid misclassification (a total area of approximately 10.14 ha).

To further validate the upscaling from high resolution UAV imagery to satellite time series, we compared the LSTM predictions with fractional cover values obtained from an aerial orthophoto (GSD = 20 cm) for the Saxon Switzerland National Park, which was not part of model training and validation. Therefore, we semi-automatically classified the standing deadwood in the orthophoto (i.e., red-green band ratio, thresholding, manual refinement), calculated the fractional cover of standing deadwood with the superimposed Sentinel-2 grid, and compared it with the LSTM predictions. All analyses were conducted in R language (R Core Team, 2022) and the code is available are https://github.com/FelixSchiefer/TreeMortality. Landscape-level prediction maps for Germany are available at https://doi.org/10.5445/IR/1000155244 and will be continuously expanded.

3. Results

3.1. CNN-based deadwood segmentation in UAV-orthomosaics (local level)

The CNN-based segmentation of standing deadwood in the UAV imagery was very accurate with precision = 0.9, recall = 0.82, and F1-score = 0.85 derived from the five-fold block cross-validation (Fig. 4a). Model performance was relatively consistent across all study sites, as shown by the median F1-score of 0.82 (interquartile range: IQR = 0.15) (Fig. 4b). Model performance was also consistent across different years, with median F1-scores of 2017: 0.79 (IQR = 0.20, n = 56), 2018: 0.66 (IQR = 0.30, n = 5), 2019: 0.82 (IQR = 0.16, n = 60), 2020: 0.81 (IQR = 0.15, n = 35), and 2021: 0.87 (IQR = 0.07, n = 20). The median F1-scores per study region were Southern Black Forest: 0.82 (IQR = 0.15), Northern Black Forest: 0.87 (IQR = 0.07), Dresden Heath: 0.87 (IQR = 0.08), Karlsruhe-Bretten: 0.61 (IQR = 0.16), Hainich National Park: 0.11 (IQR = 0), and Helsinki: 0.78 (IQR = 0.04) (see Appendix for site-specific values). Low F1-scores for standing deadwood were mainly observed at sites with very low area-related proportions of standing deadwood and at sites where the UAV acquisition was very late in the growing season (e.g., Hainich National Park). For the latter, deciduous trees that had already shed some of their foliage were partly misclassified as standing deadwood. Low F1-scores together with low precision but high recall were observed for sites where there were many dead branches on the forest floor after very recent logging, which could easily be mistaken for standing deadwood.

3.2. Mapping fractional cover of standing deadwood from sentinel time series using LSTM (landscape level)

Fig. 5 shows the Pearson's correlation coefficient (r) and the slope value of the total least squares (TLS) regressions for the different input band sets to the LSTM models. The highest median r value (0.62) was observed for the S2+VI input band set with 12 Sentinel-2 bands from the five times repeated ten-fold block cross-validation. Total least squares regression slope values closest to 1 were observed for the S1+S2+VI input band set but with all available Sentinel-2 bands (median slope = 1.56). In general, additional information from Sentinel-1 alone (i.e., backscatter and interferometric coherence) reduced model performance compared to the models using only Sentinel-2 data. Contrary, model performance increased when vegetation indices (i.e., kNDVI and NDWI) were added to the Sentinel-2 data. Using all available input band sets especially improved the regression slope values. LSTM model

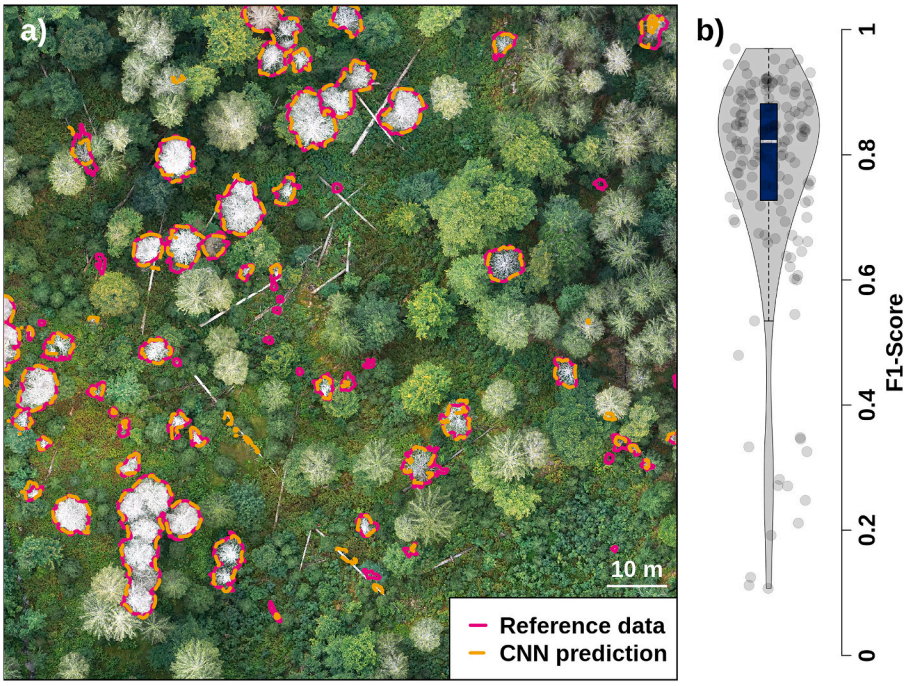

Fig. 4. a) Illustration of the CNN model performance for the semantic segmentation of standing deadwood in UAV orthoimagery for a Southern Black Forest site. (Coordinate reference system: WGS84/UTM zone 32N, EPSG:32632). b) Distribution of F1-score values across study sites from the five-fold block cross-validation.

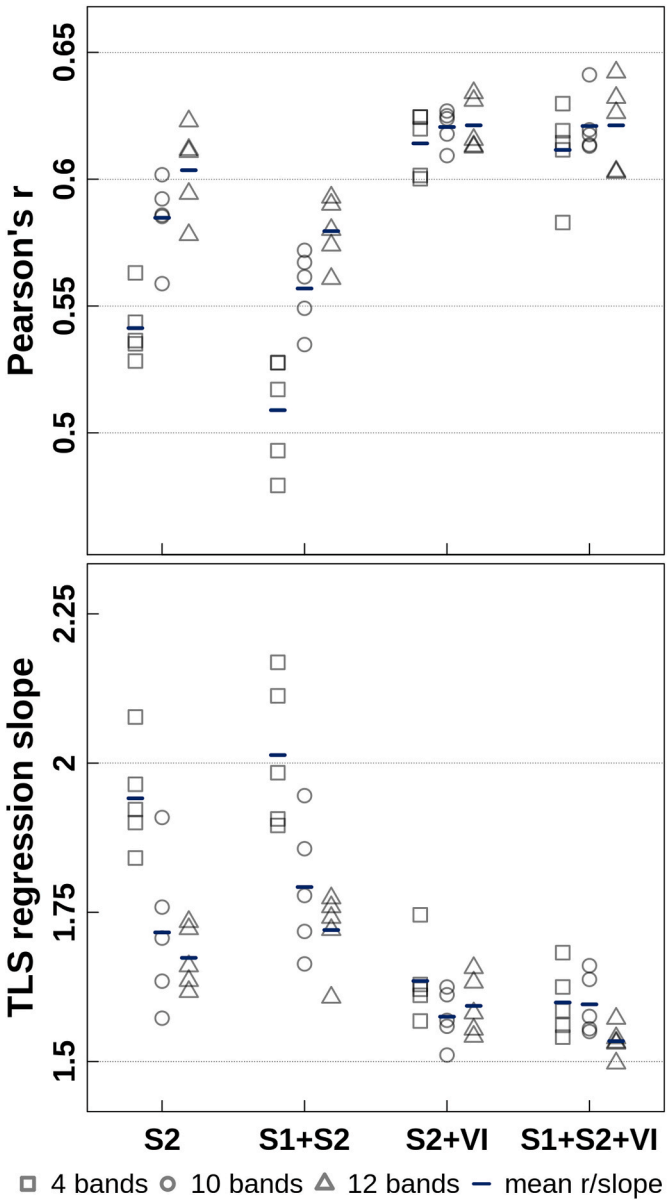

Fig. 5. Pearson's r (upper panel) and total least squares regression slope (lower panel) of the five times repeated ten-fold cross-validations of the LSTM models for different inputs of Sentinel-1 and Sentinel-2 band sets (S2: Sentinel-2; S1+S2: Sentinel-1 and Sentinel-2; S2+VI; Sentinel-2, kNDVI, and NDWI; S1+S2+VI: Sentinel-1, Sentinel-2, kNDVI, and NDWI), each with different Sentinel-2 bands (4: 10 m bands; 10: 10 & 20 m bands; 12: 10, 20 & 60 m bands).

performance increased with more spectral information from the 20 m Sentinel-2 bands (i.e., 10 bands) and even more with the 20 m and 60 m Sentinel-2 bands (i.e., 12 bands).

Based on the TLS slope value closest to 1 (slope = 1.58, Pearson's r = 0.66), the LSTM model with the S1+S2+VI and 12 Sentinel-2 bands input band set was selected for landscape-level predictions (Fig. 6). Uncertainties in the predictions were evenly distributed across the entire value range (Fig. 6), except for observed values close to 0 and 1, where we observed overpredictions near 0 and underpredictions near 1. Model performance was stable across the study regions with RMSE values for the Southern Black Forest: 0.21, Northern Black Forest: 0.21, Dresden Heath: 0.22, Karlsruhe-Bretten: 0.23, Hainich National Park: 0.21, and Helsinki: 0.19 (see Appendix for site-specific values).

Fig. 7 shows the Sentinel-based prediction map of standing deadwood cover for the year 2020 using the previously selected best-performing LSTM model (S1+S2+VI with 12 Sentinel-2 bands) exemplarily for the Saxon Switzerland National Park and its surroundings in Germany. The latter was largely affected by the drought events of 2018 and 2019 and thus provides a suitable test region with large gradients in deadwood cover. As expected, the map overview (center) reveals ample occurrences of tree mortality in the National Park, with 24.1% of the Sentinel pixels showing more than 50% standing deadwood cover and 6.6% of the pixels showing more than 75% standing deadwood cover. As can be seen in comparison with independently acquired aerial orthoimagery in the close-up panels (top and bottom), crown cover of standing deadwood was accurately predicted from Sentinel data with a high spatial detail (10 m spatial resolution).

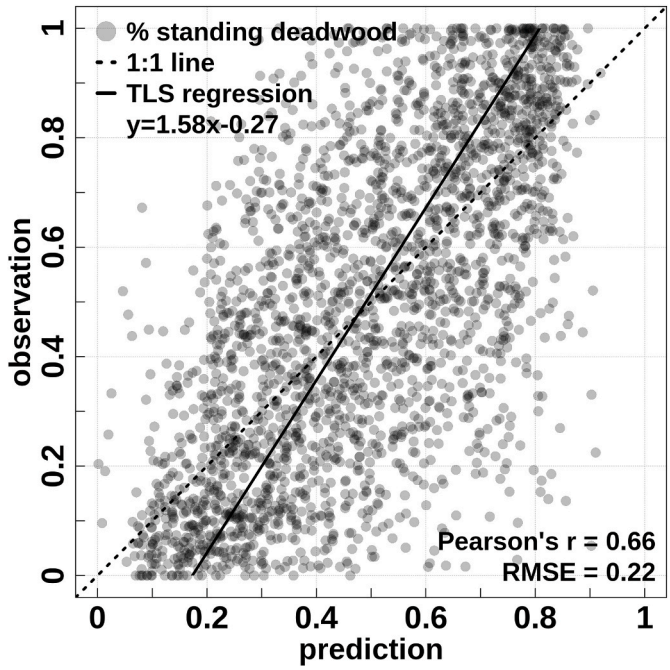

Fig. 6. Scatterplot of observed and predicted fractional cover values of standing deadwood [%] at landscape level from the selected LSTM model (S1+S2+VI, 12 Sentinel-2 bands). Each dot represents a 10 m Sentinel-2 pixel with reference data available from the UAV-based segmentation.

Annual LSTM prediction maps of standing deadwood cover in an example region in the Saxon Switzerland National Park for the years 2018–2021 are shown in Fig. 8. The lower left panel displays histograms of fractional cover values of standing deadwood for each year between 2018 and 2021. After an initial crown dieback in 2018, most of the area was affected by tree mortality in 2019. The number of pixels classified with high fractions of standing deadwood subsequently decreased in the years 2020 and 2021. In the same years, more pixels with small values of standing deadwood cover can be observed in the histogram and are also apparent in the LSTM prediction maps as dark blue patches.

4. Discussion

4.1. UAV- and CNN-based deadwood segmentation as a reference data source

With an F1-score of 0.85 from independent five-fold block cross-validation, the automated segmentation of standing deadwood in UAV imagery based on CNN models was confirmed to be very accurate. The very low median F1-score for the Hainich National Park sites (0.11) can be explained by the small proportion of standing deadwood for the respective sites, since even small areas can have a large relative effect on the model results (e.g., small branches that were classified as deadwood

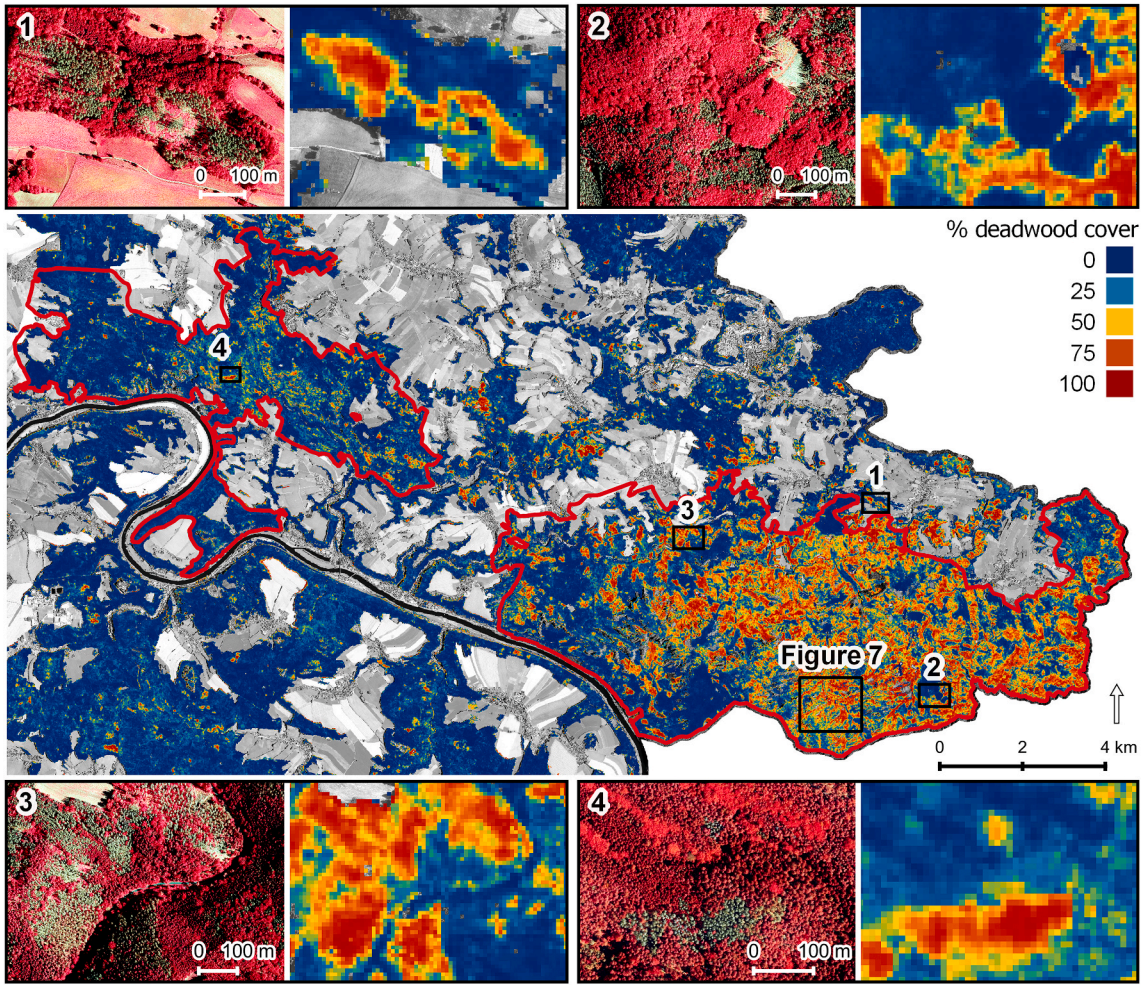

Fig. 7. Sentinel-based LSTM prediction map of fractional standing deadwood cover for the year 2020 in Saxon Switzerland National Park (red outline), Germany (Coordinate reference system: WGS84/UTM zone 33N, EPSG:32633; center coordinates: 450795.3, 5638435.7). Close-ups in the panels show amplified examples of forest condition in Color infrared-orthophotos (Staatsbetrieb Geobasisinformation und Vermessung Sachsen, GeoSN) and corresponding prediction maps.

but were not labeled as such in the reference data due to their small size). It should be noted that the model performance is based on reference data derived from a human interpreter. While the generation of reference data from visual interpretation of high-resolution imagery is a very common approach, it also comes with uncertainties that may likely result in an underestimation of the model performance (Kattenborn et al., 2021). Consistent with our results, Sylvain et al. (2019) reported an F1-score of 0.95 for classifying tree health status (live or dead trees) using a VGG16 CNN on RGB aerial photos (20 cm GSD) over 990 1 ha sites in south-central Quebec, Canada. Jiang et al. (2019) also reported very high accuracies for the segmentation of standing dead trees using an FCN-DenseNet CNN, based on two airborne color-infrared orthomosaics (20 cm GSD) from the Bavarian Forest National Park, Germany. Sani-Mohammed et al. (2022) used a Mask R-CNN for an instance segmentation of standing dead trees from an airborne color-infrared orthomosaic (20 cm GSD) over the Bavarian Forest National Park, Germany, and reported an F1-score of 0.87. Yet, the dataset used here likely comprises a higher variability in site and data conditions than in the aforementioned studies. In this study, the RGB-orthomosaics were acquired in six study regions over 176 sites that differ in forest stand composition and structure. Imagery was acquired with different drone platforms and sensors and at different times of the day over a five-year period, resulting in very different sun-sensor geometries and environmental and atmospheric conditions. Given this heterogeneity of the dataset, our results show that the CNN-based segmentation of standing deadwood was spatially and temporally robust and that the CNN models generalized well.

While the present study focuses solely on RGB imagery due to its relative ease of acquisition and wide availability, other sensor types are also commonly used for dead tree detection, including multispectral (Jiang et al., 2019; Meddens et al., 2011; Sani-Mohammed et al., 2022; Zielewska-Büttner et al., 2020), hyperspectral (Einzmann et al., 2021; Fricker et al., 2019), and LiDAR (Briechle et al., 2021; Hell et al., 2022). While higher spectral resolution remote sensing data may be advantageous for separating spectrally similar classes (e.g., tree species), we have shown that RGB data are sufficient for separating live and dead trees in very high-resolution UAV imagery. It should be noted, however, that we only defined dead trees or trees with clear signs of dieback or foliage discoloration as deadwood and that we did not consider early stages of tree mortality (e.g., green attack following bark beetle infestation). Alternative detection methods, such as instance segmentation (Chiang et al., 2020; Sani-Mohammed et al., 2022) or object detection (Safonova et al., 2019, 2022) would even allow to map tree individuals. However, this would not have added value to this study, because for the landscape-level upscaling we targeted the fractional cover of deadwood per Sentinel-2 pixel rather than the number of dead trees. An instance segmentation approach would have further complicated the labeling of reference data and increased model complexity (see review by Hoeser and Kuenzer, 2020).

An often-reported problem in deadwood detection tasks is the

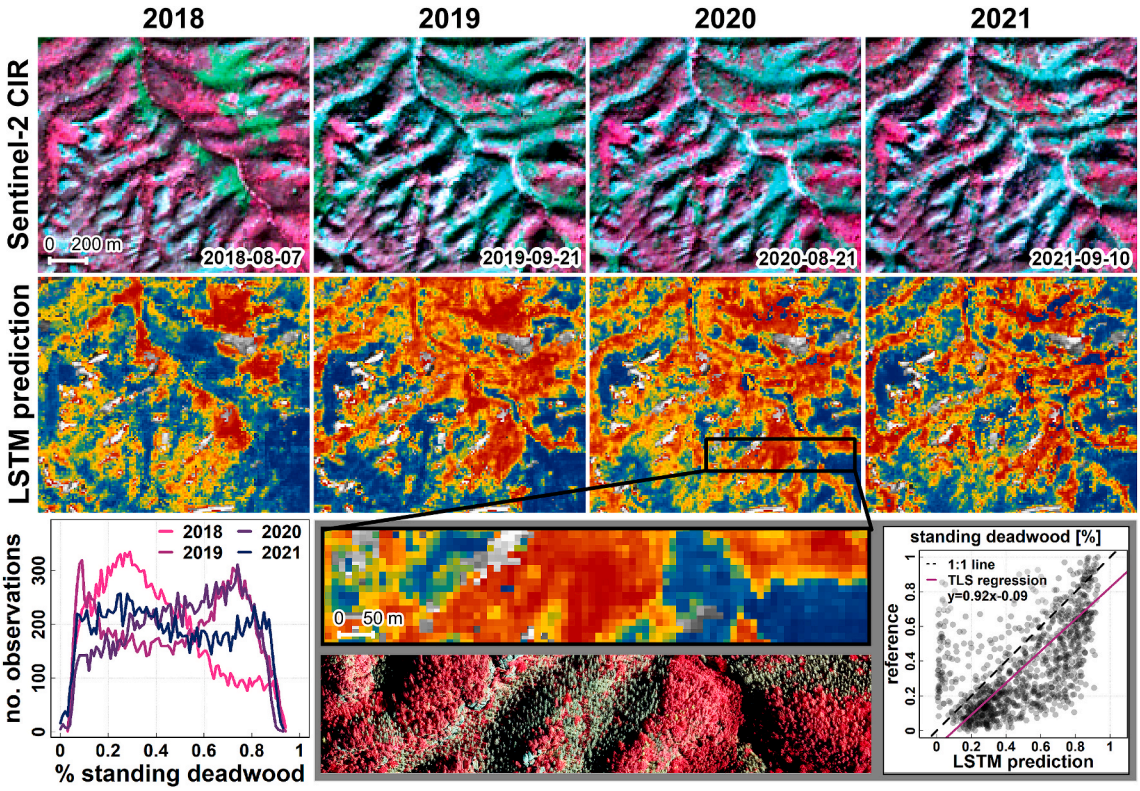

Fig. 8. Sentinel-2 Color infrared image (CIR; top row; R = B8, G = B3, B—B2) and LSTM prediction maps of standing deadwood cover (center row) in an example region in Saxon Switzerland National Park (see Fig. 7 for the extent) across the years 2018, 2019, 2020, and 2021 (Coordinate reference system: WGS84/UTM zone 33N, EPSG:32633; center coordinates: 444628, 5643575). The histogram shows the standing deadwood cover values for each year. The grey box shows an independent validation of the LSTM predictions based on fractional cover values derived from an aerial orthophoto. Source CIR-orthophoto: Staatsbetrieb Geobasisinformation und Vermessung Sachsen (GeoSN).

difficulty in separating deadwood from bare ground (Fassnacht et al., 2014; Meddens et al., 2011; Zielewska-Büttner et al., 2020). While these findings have primarily been reported for pixel-based classification algorithms, we did not encounter substantial misclassifications in the CNN-based deadwood segmentation, suggesting that high-resolution textures are sufficient to separate bare ground from dead trees. For the time series-based upscaling approach, we added reference data from open forest floor and areas with sparse herbaceous vegetation. LSTM model performances clearly improved compared to an LSTM without these additional data (results not shown).

Overall, the described procedure can be used as an effective tool for rapid generation of reference data for large areas. This not only fosters research in remote or inaccessible areas, but also allows for the collection of larger amounts of reference data than field-based data collection would allow. The models can also be used to continuously append reference datasets with predictions from newly acquired orthomosaics, despite varying site and scene characteristics (e.g., environmental and atmospheric conditions, sun-sensor geometry). In this context, it is important to note that there are several platforms that curate openly available UAV orthoimagery (mostly RGB data) contributed by research groups or citizen scientists (e.g., geonadir.com, opendrop.de or openaerialmap.org). In combination with the described CNN-based methods, these databases and their spatiotemporal coverage can greatly stimulate the potential of using UAV-based reference data for satellite-based applications (Kattenborn et al., 2019).

4.2. LSTM-based modeling of standing deadwood from satellite time series

Our results from the LSTM-based modeling of standing deadwood showed that using all available spectral information from Sentinel-2 increased model performance. We observed the highest model performance (according to TLS-regression slope) when integrating all spectral bands from Sentinel-2, Sentinel-1 backscatter and interferometric coherence, and the vegetation indices kNDVI and NDWI. While it is generally assumed that neural networks do not require pronounced feature engineering, our results indicate that adding vegetation indices to the raw spectral information can further refine the model. This may be explained by the fact that vegetation indices are often based on physical principles (e.g., NDVI as a ratio of light absorption and scattering). Indirectly incorporating such physical consistency may constrain the complexity of a model and facilitate the learning process (Reichstein et al., 2019). While Sentinel-1 information alone decreased model performance when added to the Sentinel-2 bands (S1+S2), incorporating physical constraints into the model by means of vegetation indices (S1+S2+VI) also allowed the radar information to be used and thus showed the best model performance. At first glance, LSTM model performance in upscaling, with a Pearson's r of 0.66 and an RMSE of 22% (S1+S2+VI), may not appear very high. Nevertheless, we consider these model performances promising considering the following aspects:

Standing deadwood may appear very differently for different species and also for different stand characteristics. For instance, the different growth forms of broadleaf and needleleaf trees not only have different textural and spectral characteristics of healthy tree individuals but are also reflected in the appearance of dead tree crowns, complicating the modeling task. Different temporal signatures (e.g., deciduous and evergreen species) may further add complexity to the model, although little is known about this effect and its interactions with the textural and spectral properties. Moreover, in the UAV-based reference data acquisition, standing dead tree crowns were segmented by an area corresponding to a convex hull of the branches (see Fig. 4). Thus, due to gaps within branches or holes in the canopy, the segmented canopy area may

not exactly match the true cover of a dead tree crown, and thus the relationship between cover and reflectance signals may be compromised. This effect adds even more complexity when dense understory distinctly shines through the dead tree crowns (Frolking et al., 2009), which further constrains the isolation of unique spectral features of dead tree crowns in an already subtle process of non-stand replacing tree mortality. Thus, the task of mapping dead tree crowns may appear more trivial than it actually is, particularly for large environmental gradients.

Other studies have attempted to map tree mortality at landscape-level using upscaling approaches from high-resolution aerial images to coarser-resolution Landsat imagery (Campbell et al., 2020; Hart and Veblen, 2015; Meddens et al., 2013; Schwantes et al., 2016). Reported accuracies for the local-level predictions were comparably high but required more sophisticated input data (e.g., additional LiDAR data) or (pre)processing than the UAV RGB imagery and the end-to-end learning CNNs used here. Although these studies reported higher accuracies for landscape-level predictions, comparison of the results is limited because the coarser resolution of Landsat hardly accounts for subtle and small-scale deadwood occurrences and because of different definitions of deadwood (e.g., grey stage was excluded in Meddens et al. (2013)).

Model performance was estimated using spatial block cross-validation, where each individual site with available UAV data was treated as a block during the cross-validation. Although several methods have been recommended to alleviate optimistically biased model performance (Burman et al., 1994; Roberts et al., 2017), recent studies suggest that spatial dependence in the raw data is often overlooked (Ploton et al., 2020). This is particularly the case in deep learning-based studies, where random cross-validation schemes prevail and spatial independence between training and validation data is not always ensured (Kattenborn et al., 2022). Thus, the model performance assessed in this study may not be directly comparable to similar approaches using other biased validation schemes that do not account for the spatial dependence between training and test datasets. It should also be noted that the model performance was tested across years and regions, while growing seasons, and thus temporal patterns of the spectral signatures, may largely deviate across time and space (Hufkens et al., 2012; Verbesselt et al., 2010).

Linking the two data sources is essential for model training, so the data must be spatially and temporally matched. Reference data from UAV orthomosaics were acquired throughout the entire growing season (April to November), while the end of a satellite time series was set to October 30 of the respective year. Setting a specific end date was motivated by the LSTM modeling, which is facilitated by equidistant and synchronized time series. Consequently, a standing dead tree crown visible in a UAV scene was considered to be dead for the entire year of the acquisition. However, this may not be completely true for all observations, and such temporal mismatches may further reduce the estimated model performance.

In addition to a temporal mismatch between UAV and Sentinel data, a spatial mismatch can also hinder model training and reduce model performance estimates. In this regard, spatially more accurate UAV acquisitions using real-time kinematic (RTK) GNSS data may be very promising (not available in this study). However, it should be noted that RTK base stations are not always easy to deploy in forest environments, and RTK-based surveys only improve the absolute positional accuracy of the UAV data. A spatial mismatch between UAV and satellite data may remain, as the absolute geolocation accuracy of, for example, Sentinel-2 is specified at 12.5 m (Gascon et al., 2017). Additionally, automatic co-registration methods, such as Scale-Invariant Feature Transform (Lowe, 2004), are not suitable for remote sensing data with very different spatial resolutions, since the extracted image features will not be found in both images. Therefore, we tested a simple optimization method that co-registers resampled UAV imagery and the Sentinel-2 RGB-bands by iteratively shifting and rotating the UAV data and finding the maximum correlation of the spectral bands available in both datasets (i.e., red, green, and blue). Gränzig et al. (2021) presented a similar optimization approach where the optimal position is determined by the optimal fit between UAV-derived land cover fractions and Sentinel-2 spectral information. Independent validation of such optimization methods is difficult outside of dedicated experiments, and we assumed the method to be valid if the LSTM model performance improved in the upscaling approach. Contrary to our assumption, the LSTM model performance did not improve (presumably due to the different UAV acquisition times compared to the constant Sentinel-2 overpass time and the resulting differences in lighting situation and shadows), and we decided to discard the co-registration approach in this study. Yet, future studies may address the co-registration problem to further improve the potential of the presented approach.

Despite the presented sources of uncertainty, our results indicate a high transferability across the individual study regions with evenly distributed RMSE values ranging from 0.23 for the Karlsruhe-Bretten region to 0.19 for Helsinki. An independent comparison between the extrapolations and aerial orthophotos in space (Fig. 7) and time (Fig. 8) also suggests a robust and consistent predictive performance of the LSTM model. Time series approaches are particularly useful for capturing dynamic processes such as tree mortality, since a static selection of acquisition dates introduces selection bias and hence uncertainty (Frantz et al., 2022). For instance, after disturbance, increased light availability on the ground facilitates rapid (re)growth and greening of understory vegetation (Frolking et al., 2009; Meng et al., 2018). In addition, visibility of the understory from a bird's-eye perspective is enhanced by the sparse canopies of standing dead trees (particularly for deciduous trees). Modeling approaches based on single image acquisitions might easily confuse this regrown understory with a vital overstory. Time series approaches, on the other hand, capture the context and dynamics prior to canopy mortality and should detect canopy mortality more robustly.

The LSTM is specifically designed to detect temporal features of tree mortality throughout the time series and to indicate whether standing deadwood was present in the year of interest. This might be particularly relevant under common forest management practices (i.e., salvage logging and sanitation harvest after disturbance), where standing dead trees may have already been removed and thus may be missed by single time-step algorithms. For example, it is possible that standing dead wood has already been removed by foresters (e.g., for timber usage or path safety), but the algorithm can still detect the temporal presence of standing deadwood based on corresponding features in a period of the time series. Thus, the presented time series-based approach is also capable of detecting rapidly evolving and short-lived occurrences of standing deadwood.

An often-reported advantage of deep neural networks are their end-to-end learning capabilities without the need of enhanced preprocessing steps. In this study, the preprocessing for the LSTM modeling was confined to linear interpolation of missing values in the satellite time series and cloud masking. Results from Ruβwurm and Körner (2018) indicate that the latter can be learned jointly with the classification task, further reducing preprocessing. Thus, in concert with cloud platforms where massive amounts of raw satellite data are stored (e.g., DIAS, Google Earth Engine), models may be trained that indirectly learn data quality features and transformations analogous to data preprocessing, which in turn could enhance the data processing efficiency and robustness for applications over large spatial and temporal scales.

In this study, we demonstrated the upscaling from standing deadwood segmentation maps at local-level (centimeter range) to continuous cover fractions at coarser resolution (10 m resolution) and large areas by combining pattern recognition in UAV imagery and satellite time series analysis. This approach exploits both the high spatial information of UAV imagery and the high spectral and temporal information of satellite data. The quantitative performance assessment using spatially explicit validation data (Fig. 6) as well as the continuous and multi-temporal prediction maps (Fig. 7) showed that the predicted continuous cover fractions do not only resemble large-scale tree mortality rates (e.g., of

entire forest stands), but also robustly predict transitions of tree mortality cover fractions or scattered occurrences at small spatial scales. The fractional cover maps presented here do specifically reflect the presence of dead trees, but do not indicate other sources of forest loss, e.g., due to logging or intense forest fires. This can be particularly important for monitoring the typically widespread and patchy patterns of tree mortality events associated with climate extremes such as drought, disease, pathogens, and their combined effects.

5. Conclusion

Spatio-temporal information on forest mortality and associated processes is scarce, but urgently needed for understanding climate change risks on forests. Earth observation satellites could provide spatially and temporally explicit information on tree mortality, but mapping tree mortality with such data requires ample training data. In this study, we presented a workflow that enables large-scale mapping of tree mortality. The automated generation of reference data from high-resolution UAV imagery enables spatially explicit training and validation of landscape-level models, which is hardly possible with most existing reference data sources. Opportunities for optimization exist, particularly regarding the spatial and temporal consistency between UAV and satellite products, and the representation of natural variability in the appearance of dead tree crowns in corresponding remote sensing signals and should be subject to further research. Precise estimates of fractional cover of standing deadwood could be used with other products, e.g., biomass estimates, canopy height, or species maps, to estimate tree mortality-related changes in carbon dynamics. Deadwood is also an important forest structural parameter and large-scale continuous information on its fractional cover may foster forest biodiversity research and management. With the appropriate UAV data for reference data generation, the approach can be adapted to a wide range of applications in vegetation remote sensing (e.g., tree species or habitat mapping). In the future, the increasing availability of openly available UAV data in concert with automated and transferable deep learning-based mapping algorithms will further increase the potential of such multi-scale approaches.

CRediT authorship contribution statement

Felix Schiefer: Methodology, Software, Validation, Formal Analysis, Investigation, Data Curation, Writing - Original Draft, Writing - Review & Editing, Visualization. **Annett Frick:** Conceptualization, Validation, Resources, Writing - Review & Editing. **Julian Frey:** Investigation, Data Curation. **Randolf Klinke:** Validation. **Katarzyna Zielewska-Büttner:** Writing - Review & Editing. **Andreas Uhl:** Investigation, Data Curation. **Samuli Junttila:** Investigation, Writing - Review & Editing. **Sebastian Schmidtlein:** Resources, Writing - Review & Editing. **Teja Kattenborn:** Conceptualization, Methodology, Writing - Original Draft, Writing - Review & Editing, Supervision, Funding acquisition.

Declaration of competing interest

The authors declare that they have no known competing financial interests or personal relationships that could have appeared to influence the work reported in this paper.

Acknowledgements

The study has been funded by the German Aerospace Centre (DLR) on behalf of the Federal Ministry for Economic Affairs and Climate Action (BMWK) [FKZ 50EE1909A]. The data acquisition within the Southern Black Forest was funded by the German Research Foundation DFG [GRK 2123]. SJ was funded through the Academy of Finland under grants [330422, 337127]. We thank the 3DGeo Research Group at Heidelberg University for the provision of UAV imagery from the Karlsruhe-Bretten study site and the Forest Research Institute Baden-Württemberg (FVA) and Black Forest National Park for the provision of UAV imagery from the Black Forest. We acknowledge support by the KIT-Publication Fund of the Karlsruhe Institute of Technology.

Appendix A. Supplementary data

Supplementary data to this article can be found online at https://doi.org/10.1016/j.ophoto.2023.100034.

References

Ali, A.M., Abdullah, H., Darvishzadeh, R., Skidmore, A.K., Heurich, M., Roeoesli, C., Paganini, M., Heiden, U., Marshall, D., 2021. Canopy chlorophyll content retrieved from time series remote sensing data as a proxy for detecting bark beetle infestation. Remote Sens. Appl. Soc. Environ. 22, 100524 https://doi.org/10.1016/j.rsase.2021.100524.

Allen, C.D., Macalady, A.K., Chenchouni, H., Bachelet, D., McDowell, N., Vennetier, M., Kitzberger, T., Rigling, A., Breshears, D.D., Hogg, E.H., Ted), Gonzalez, P., Fensham, R., Zhang, Z., Castro, J., Demidova, N., Lim, J.-H., Allard, G., Running, S. W., Semerci, A., Cobb, N., 2010. A global overview of drought and heat-induced tree mortality reveals emerging climate change risks for forests. For. Ecol. Manag., Adaptation of Forests and Forest Management to Changing Climate 259, 660–684. https://doi.org/10.1016/j.foreco.2009.09.001.

Alvarez-Vanhard, E., Corpetti, T., Houet, T., 2021. UAV & satellite synergies for optical remote sensing applications: a literature review. Sci. Remote Sens. 3, 100019 https://doi.org/10.1016/j.srs.2021.100019.

Bárta, V., Lukeš, P., Homolová, L., 2021. Early detection of bark beetle infestation in Norway spruce forests of Central Europe using Sentinel-2. Int. J. Appl. Earth Obs. Geoinformation 100, 102335. https://doi.org/10.1016/j.jag.2021.102335.

Bastos, A., Orth, R., Reichstein, M., Ciais, P., Viovy, N., Zaehle, S., Anthoni, P., Arneth, A., Gentine, P., Joetzjer, E., Lienert, S., Loughran, T., McGuire, P.C., O, S., Pongratz, J., Sitch, S., 2021. Vulnerability of European ecosystems to two compound dry and hot summers in 2018 and 2019. Earth Syst. Dyn. 12, 1015–1035. https://doi.org/10.5194/esd-12-1015-2021.

Breiman, L., 2001. Random forests. Mach. Learn. 45, 5–32, 10/d8zjwq.

Briechle, S., Krzystek, P., Vosselman, G., 2021. Silvi-Net – a dual-CNN approach for combined classification of tree species and standing dead trees from remote sensing data. Int. J. Appl. Earth Obs. Geoinformation 98, 102292. https://doi.org/10.1016/j.jag.2020.102292.

Buras, A., Rammig, A., Zang, C.S., 2020. Quantifying impacts of the 2018 drought on European ecosystems in comparison to 2003. Biogeosciences 17, 1655–1672, 10/ggqkhm.

Burman, P., Chow, E., Nolan, D., 1994. A cross-validatory method for dependent data. Biometrika 81, 351–358. https://doi.org/10.2307/2336965.

Campbell, M.J., Dennison, P.E., Tune, J.W., Kannenberg, S.A., Kerr, K.L., Codding, B.F., Anderegg, W.R.L., 2020. A multi-sensor, multi-scale approach to mapping tree mortality in woodland ecosystems. Remote Sens. Environ. 245, 111853 https://doi.org/10.1016/j.rse.2020.111853.

Camps-Valls, G., Campos-Taberner, M., Moreno-Martínez, Á., Walther, S., Duveiller, G., Cescatti, A., Mahecha, M.D., Muñoz-Marí, J., García-Haro, F.J., Guanter, L., Jung, M., Gamon, J.A., Reichstein, M., Running, S.W., 2021. A unified vegetation index for quantifying the terrestrial biosphere. Sci. Adv. 7, eabc7447 https://doi.org/10.1126/sciadv.abc7447.

Chiang, C.-Y., Barnes, C., Angelov, P., Jiang, R., 2020. Deep learning-based automated forest health diagnosis from aerial images. IEEE Access 8, 144064–144076. https://doi.org/10.1109/ACCESS.2020.3012417.

Coops, N.C., Shang, C., Wulder, M.A., White, J.C., Hermosilla, T., 2020. Change in forest condition: characterizing non-stand replacing disturbances using time series satellite imagery. For. Ecol. Manag. 474, 118370 https://doi.org/10.1016/j.foreco.2020.118370.

Einzmann, K., Atzberger, C., Pinnel, N., Glas, C., Böck, S., Seitz, R., Immitzer, M., 2021. Early detection of spruce vitality loss with hyperspectral data: results of an experimental study in Bavaria, Germany. Remote Sens. Environ. 266, 112676 https://doi.org/10.1016/j.rse.2021.112676.

Fassnacht, F.E., Latifi, H., Ghosh, A., Joshi, P.K., Koch, B., 2014. Assessing the potential of hyperspectral imagery to map bark beetle-induced tree mortality. Remote Sens. Environ. 140, 533–548. https://doi.org/10.1016/j.rse.2013.09.014.

Frantz, D., Hostert, P., Rufin, P., Ernst, S., Röder, A., van der Linden, S., 2022. Revisiting the past: replicability of a historic long-term vegetation dynamics assessment in the era of big data analytics. Rem. Sens. 14, 597, 10/gpcf37.

Fricker, G.A., Ventura, J.D., Wolf, J.A., North, M.P., Davis, F.W., Franklin, J., 2019. A convolutional neural network classifier identifies tree species in mixed-conifer forest from hyperspectral imagery. Rem. Sens. 11, 2326, 10/gh3dqv.

Frolking, S., Palace, M.W., Clark, D.B., Chambers, J.Q., Shugart, H.H., Hurtt, G.C., 2009. Forest disturbance and recovery: a general review in the context of spaceborne remote sensing of impacts on aboveground biomass and canopy structure. J. Geophys. Res. Biogeosciences 114. https://doi.org/10.1029/2008JG000911.

Gao, B., 1996. NDWI—a normalized difference water index for remote sensing of vegetation liquid water from space. Remote Sens. Environ. 58, 257–266. https://doi.org/10.1016/S0034-4257(96)00067-3.

Gascon, F., Bouzinac, C., Thépaut, O., Jung, M., Francesconi, B., Louis, J., Lonjou, V., Lafrance, B., Massera, S., Gaudel-Vacaresse, A., Languille, F., Alhammoud, B., Viallefont, F., Pflug, B., Bieniarz, J., Clerc, S., Pessiot, L., Trémas, T., Cadau, E., De Bonis, R., Isola, C., Martimort, P., Fernandez, V., 2017. Copernicus sentinel-2A calibration and products validation status. Rem. Sens. 9, 584. https://doi.org/10.3390/rs9060584.

Glenn, E.P., Huete, A.R., Nagler, P.L., Nelson, S.G., 2008. Relationship between remotely-sensed vegetation indices, canopy attributes and plant physiological processes: what vegetation indices can and cannot tell us about the landscape. Sensors 8, 2136–2160. https://doi.org/10.3390/s8042136.

Gränzig, T., Fassnacht, F.E., Kleinschmit, B., Förster, M., 2021. Mapping the fractional coverage of the invasive shrub Ulex europaeus with multi-temporal Sentinel-2 imagery utilizing UAV orthoimages and a new spatial optimization approach. Int. J. Appl. Earth Obs. Geoinformation 96, 102281, 10/gh3ctq.

Hammond, W.M., Williams, A.P., Abatzoglou, J.T., Adams, H.D., Klein, T., López, R., Sáenz-Romero, C., Hartmann, H., Breshears, D.D., Allen, C.D., 2022. Global field observations of tree die-off reveal hotter-drought fingerprint for Earth's forests. Nat. Commun. 13, 1761. https://doi.org/10.1038/s41467-022-29289-2.

Hansen, M.C., Potapov, P.V., Moore, R., Hancher, M., Turubanova, S.A., Tyukavina, A., Thau, D., Stehman, S.V., Goetz, S.J., Loveland, T.R., Kommareddy, A., Egorov, A., Chini, L., Justice, C.O., Townshend, J.R.G., 2013. High-resolution global maps of 21st-century forest cover change. Science 342, 850–853, 10/f5h5c2.

Hart, S.J., Veblen, T.T., 2015. Detection of spruce beetle-induced tree mortality using high- and medium-resolution remotely sensed imagery. Remote Sens. Environ. 168, 134–145. https://doi.org/10.1016/j.rse.2015.06.015.

Hartmann, H., Bastos, A., Das, A.J., Esquivel-Muelbert, A., Hammond, W.M., Martínez-Vilalta, J., McDowell, N.G., Powers, J.S., Pugh, T.A.M., Ruthrof, K.X., Allen, C.D., 2022. Climate change risks to global forest health: emergence of unexpected events of elevated tree mortality worldwide. Annu. Rev. Plant Biol. 73, 673–702. https://doi.org/10.1146/annurev-arplant-102820-012804.

Hartmann, H., Schuldt, B., Sanders, T.G.M., Macinnis-Ng, C., Boehmer, H.J., Allen, C.D., Bolte, A., Crowther, T.W., Hansen, M.C., Medlyn, B.E., Ruehr, N.K., Anderegg, W.R. L., 2018. Monitoring global tree mortality patterns and trends. Report from the VW symposium 'Crossing scales and disciplines to identify global trends of tree mortality as indicators of forest health. New Phytol. 217, 984–987, 10/gn93j8.

Hell, M., Brandmeier, M., Briechle, S., Krzystek, P., 2022. Classification of tree species and standing dead trees with lidar point clouds using two deep neural networks: PointCNN and 3DmFV-net. PFG – J. Photogramm. Remote Sens. Geoinformation Sci. 90, 103–121. https://doi.org/10.1007/s41064-022-00200-4.

Hochreiter, S., Schmidhuber, J., 1997. Long short-term memory. Neural Comput. 9, 1735–1780. https://doi.org/10.1162/neco.1997.9.8.1735.

Hoeser, T., Kuenzer, C., 2020. Object detection and image segmentation with deep learning on Earth observation data: a review-Part I: evolution and recent trends. Rem. Sens. 12, 1667. https://doi.org/10.3390/rs12101667.

Huang, J., Kautz, M., Trowbridge, A.M., Hammerbacher, A., Raffa, K.F., Adams, H.D., Goodsman, D.W., Xu, C., Meddens, A.J.H., Kandasamy, D., Gershenzon, J., Seidl, R., Hartmann, H., 2020. Tree defence and bark beetles in a drying world: carbon partitioning, functioning and modelling. New Phytol. 225, 26–36. https://doi.org/10.1111/nph.16173.

Hufkens, K., Friedl, M., Sonnentag, O., Braswell, B.H., Milliman, T., Richardson, A.D., 2012. Linking near-surface and satellite remote sensing measurements of deciduous broadleaf forest phenology. Remote Sens. Environ., Remote Sensing of Urban Environments 117, 307–321. https://doi.org/10.1016/j.rse.2011.10.006.

Jiang, S., Yao, W., Heurich, M., 2019. Dead wood detection based on semantic segmentation of VHR aerial CIR imagery using optimized FCN-Densenet. The International Archives of the Photogrammetry, Remote Sensing and Spatial Information Sciences. Presented at the ISPRS ICWG II/III PIA19+MRSS19 - Photogrammetric Image Analysis & Munich Remote Sensing Symposium: Joint ISPRS conference XLII-2/W16, 127–133. https://doi.org/10.5194/isprs-archives-XLII-2-W16-127-2019, 18-20 September 2019, Munich, Germany, Copernicus GmbH.

Kaartinen, H., Hyyppä, J., Vastaranta, M., Kukko, A., Jaakkola, A., Yu, X., Pyörälä, J., Liang, X., Liu, J., Wang, Y., Kaijaluoto, R., Melkas, T., Holopainen, M., Hyyppä, H., 2015. Accuracy of kinematic positioning using global satellite navigation systems under forest canopies. Forests 6, 3218–3236, 10/f7v2tp.

Kattenborn, T., Leitloff, J., Schiefer, F., Hinz, S., 2021. Review on convolutional neural networks (CNN) in vegetation remote sensing. ISPRS J. Photogrammetry Remote Sens. 173, 24–49, 10/ghtrws.

Kattenborn, T., Lopatin, J., Förster, M., Braun, A.C., Fassnacht, F.E., 2019. UAV data as alternative to field sampling to map woody invasive species based on combined Sentinel-1 and Sentinel-2 data. Remote Sens. Environ. 227, 61–73, 10/ghrvsr.

Kattenborn, T., Schiefer, F., Frey, J., Feilhauer, H., Mahecha, M.D., Dormann, C.F., 2022. Spatially autocorrelated training and validation samples inflate performance assessment of convolutional neural networks. ISPRS Open J. Photogramm. Remote Sens. 5, 100018 https://doi.org/10.1016/j.ophoto.2022.100018.

Liu, X., Frey, J., Denter, M., Zielewska-Büttner, K., Still, N., Koch, B., 2021. Mapping standing dead trees in temperate montane forests using a pixel- and object-based image fusion method and stereo WorldView-3 imagery. Ecol. Indicat. 133, 108438 https://doi.org/10.1016/j.ecolind.2021.108438.

Lowe, D.G., 2004. Distinctive image features from scale-invariant keypoints. Int. J. Comput. Vis. 60, 91–110. https://doi.org/10.1023/B:VISI.0000029664.99615.94.

Main-Knorn, M., Pflug, B., Louis, J., Debaecker, V., Müller-Wilm, U., Gascon, F., 2017. Sen2Cor for sentinel-2. In: Image and Signal Processing for Remote Sensing XXIII. Presented at the Image and Signal Processing for Remote Sensing XXIII. SPIE, pp. 37–48, 10/gm2trw.

Malinowski, R., Lewiński, S., Rybicki, M., Gromny, E., Jenerowicz, M., Krupiński, Michał, Nowakowski, A., Wojtkowski, C., Krupiński, Marcin, Krätzschmar, E., Schauer, P., 2020. Automated production of a land cover/use map of Europe based on sentinel-2 imagery. Rem. Sens. 12, 3523, 10/gn4z47.

McDowell, N.G., Coops, N.C., Beck, P.S.A., Chambers, J.Q., Gangodagamage, C., Hicke, J. A., Huang, C., Kennedy, R., Krofcheck, D.J., Litvak, M., Meddens, A.J.H., Muss, J., Negrón-Juarez, R., Peng, C., Schwantes, A.M., Swenson, J.J., Vernon, L.J., Williams, A.P., Xu, C., Zhao, M., Running, S.W., Allen, C.D., 2015. Global satellite monitoring of climate-induced vegetation disturbances. Trends Plant Sci. 20, 114–123, 10/f62b9j.

Meddens, A.J.H., Hicke, J.A., Vierling, L.A., 2011. Evaluating the potential of multispectral imagery to map multiple stages of tree mortality. Remote Sens. Environ. 115, 1632–1642. https://doi.org/10.1016/j.rse.2011.02.018.

Meddens, A.J.H., Hicke, J.A., Vierling, L.A., Hudak, A.T., 2013. Evaluating methods to detect bark beetle-caused tree mortality using single-date and multi-date Landsat imagery. Remote Sens. Environ. 132, 49–58. https://doi.org/10.1016/j.rse.2013.01.002.

Meng, R., Wu, J., Zhao, F., Cook, B.D., Hanavan, R.P., Serbin, S.P., 2018. Measuring short-term post-fire forest recovery across a burn severity gradient in a mixed pine-oak forest using multi-sensor remote sensing techniques. Remote Sens. Environ. 210, 282–296. https://doi.org/10.1016/j.rse.2018.03.019.

Monahan, W.B., Arnspiger, C.E., Bhatt, P., An, Z., Krist, F.J., Liu, T., Richard, R.P., Edson, C., Froese, R.E., Steffenson, J., Lammers, T.C., Frosh, R., 2022. A spectral three-dimensional color space model of tree crown health. PLoS One 17, e0272360. https://doi.org/10.1371/journal.pone.0272360.

Pause, M., Schweitzer, C., Rosenthal, M., Keuck, V., Bumberger, J., Dietrich, P., Heurich, M., Jung, A., Lausch, A., 2016. In situ/remote sensing integration to assess forest health—a review. Rem. Sens. 8, 471. https://doi.org/10.3390/rs8060471.

Ploton, P., Mortier, F., Réjou-Méchain, M., Barbier, N., Picard, N., Rossi, V., Dormann, C., Cornu, G., Viennois, G., Bayol, N., Lyapustin, A., Gourlet-Fleury, S., Pélissier, R., 2020. Spatial validation reveals poor predictive performance of large-scale ecological mapping models. Nat. Commun. 11, 4540 https://doi.org/10/ghbcv5.

R Core Team, 2022. R: A Language and Environment for Statistical Computing. R Foundation for Statistical Computing.

Reichstein, M., Camps-Valls, G., Stevens, B., Jung, M., Denzler, J., Carvalhais, N., Prabhat, 2019. Deep learning and process understanding for data-driven Earth system science. Nature 566, 195–204, 10/gfvhxk.

Roberts, D.R., Bahn, V., Ciuti, S., Boyce, M.S., Elith, J., Guillera-Arroita, G., Hauenstein, S., Lahoz-Monfort, J.J., Schröder, B., Thuiller, W., Warton, D.I., Wintle, B.A., Hartig, F., Dormann, C.F., 2017. Cross-validation strategies for data with temporal, spatial, hierarchical, or phylogenetic structure. Ecography 40, 913–929. https://doi.org/10.1111/ecog.02881.

Ronneberger, O., Fischer, P., Brox, T., 2015. U-net: convolutional networks for biomedical image segmentation. In: Navab, N., Hornegger, J., Wells, W.M., Frangi, A.F. (Eds.), Medical Image Computing and Computer-Assisted Intervention – MICCAI 2015, Lecture Notes in Computer Science. Springer International Publishing, Cham, pp. 234–241, 10/gcgk7j.

Rußwurm, M., Körner, M., 2018. Multi-temporal land cover classification with sequential recurrent encoders. ISPRS Int. J. Geo-Inf. 7, 129. https://doi.org/10.3390/ijgi7040129.

Safonova, A., Hamad, Y., Alekhina, A., Kaplun, D., 2022. Detection of Norway spruce trees (picea abies) infested by bark beetle in UAV images using YOLOs architectures. IEEE Access 10, 10384–10392. https://doi.org/10.1109/ACCESS.2022.3144433.

Safonova, A., Tabik, S., Alcaraz-Segura, D., Rubtsov, A., Maglinets, Y., Herrera, F., 2019. Detection of fir trees (abies sibirica) damaged by the bark beetle in unmanned aerial vehicle images with deep learning. Rem. Sens. 11, 643, 10/gh3dnj.

Sani-Mohammed, A., Yao, W., Heurich, M., 2022. Instance segmentation of standing dead trees in dense forest from aerial imagery using deep learning. ISPRS Open J. Photogramm. Remote Sens. 6, 100024 https://doi.org/10.1016/j.ophoto.2022.100024.

Schiefer, F., Kattenborn, T., Frick, A., Frey, J., Schall, P., Koch, B., Schmidtlein, S., 2020. Mapping forest tree species in high resolution UAV-based RGB-imagery by means of convolutional neural networks. ISPRS J. Photogrammetry Remote Sens. 170, 205–215, 10/ghrrhs.

Schuldt, B., Buras, A., Arend, M., Vitasse, Y., Beierkuhnlein, C., Damm, A., Gharun, M., Grams, T.E.E., Hauck, M., Hajek, P., Hartmann, H., Hiltbrunner, E., Hoch, G., Holloway-Phillips, M., Körner, C., Larysch, E., Lübbe, T., Nelson, D.B., Rammig, A., Rigling, A., Rose, L., Ruehr, N.K., Schumann, K., Weiser, F., Werner, C., Wohlgemuth, T., Zang, C.S., Kahmen, A., 2020. A first assessment of the impact of the extreme 2018 summer drought on Central European forests. Basic Appl. Ecol. 45, 86–103, 10/gm7jmn.

Schuster, M., Paliwal, K.K., 1997. Bidirectional recurrent neural networks. IEEE Trans. Signal Process. 45, 2673–2681. https://doi.org/10.1109/78.650093.

Schwantes, A.M., Swenson, J.J., Jackson, R.B., 2016. Quantifying drought-induced tree mortality in the open canopy woodlands of central Texas. Remote Sens. Environ. 181, 54–64. https://doi.org/10.1016/j.rse.2016.03.027.

Senf, C., Buras, A., Zang, C.S., Rammig, A., Seidl, R., 2020. Excess forest mortality is consistently linked to drought across Europe. Nat. Commun. 11, 6200, 10/gm7vhk.

Senf, C., Sebald, J., Seidl, R., 2021. Increasing canopy mortality affects the future demographic structure of Europe's forests. One Earth 4, 749–755, 10/gpg6ms.

Senf, C., Seidl, R., 2021. Mapping the forest disturbance regimes of Europe. Nat. Sustain. 4, 63–70, 10/ghbmqz.

Sylvain, J.-D., Drolet, G., Brown, N., 2019. Mapping dead forest cover using a deep convolutional neural network and digital aerial photography. ISPRS J. Photogrammetry Remote Sens. 156, 14–26. https://doi.org/10.1016/j.isprsjprs.2019.07.010.

Thonfeld, F., Gessner, U., Holzwarth, S., Kriese, J., da Ponte, E., Huth, J., Kuenzer, C., 2022. A first assessment of canopy cover loss in Germany's forests after the 2018–2020 drought years. Rem. Sens. 14, 562. https://doi.org/10.3390/rs14030562.

Trumbore, S., Brando, P., Hartmann, H., 2015. Forest health and global change. Science 349, 814–818. https://doi.org/10.1126/science.aac6759.

Valbuena, R., Mauro, F., Suárez, R.R.-S., Manzanera, J.A., 2010. Accuracy and precision of GPS receivers under forest canopies in a mountainous environment. Span. J. Agric. Res. 8, 1047–1057, 10/gh3dk4.

Verbesselt, J., Hyndman, R., Newnham, G., Culvenor, D., 2010. Detecting trend and seasonal changes in satellite image time series. Remote Sens. Environ. 114, 106–115. https://doi.org/10.1016/j.rse.2009.08.014.

White, J.C., Wulder, M.A., Hermosilla, T., Coops, N.C., Hobart, G.W., 2017. A nationwide annual characterization of 25years of forest disturbance and recovery for Canada using Landsat time series. Remote Sens. Environ. 194, 303–321, 10/gh7xmx.

Xue, J., Su, B., 2017. Significant remote sensing vegetation indices: a review of developments and applications. J. Sens. 1–17. https://doi.org/10.1155/2017/1353691, 2017.

Zielewska-Büttner, K., Adler, P., Kolbe, S., Beck, R., Ganter, L.M., Koch, B., Braunisch, V., 2020. Detection of standing deadwood from aerial imagery products: two methods for addressing the bare ground misclassification issue. Forests 11, 801, 10/gmcncf.

Zscheischler, J., Martius, O., Westra, S., Bevacqua, E., Raymond, C., Horton, R.M., van den Hurk, B., AghaKouchak, A., Jézéquel, A., Mahecha, M.D., Maraun, D., Ramos, A. M., Ridder, N.N., Thiery, W., Vignotto, E., 2020. A typology of compound weather and climate events. Nat. Rev. Earth Environ. 1, 333–347. https://doi.org/10.1038/s43017-020-0060-z.